Contribution from the Department of Chemistry,
Washington State University, Pullman, Washington 99164

Synthesis and Characterization of a Series of Novel Rhodium and Iridium Complexes Containing Polypyridyl Bridging Ligands: Potential Uses in the Development of Multimetal Catalysts for Carbon Dioxide Reduction

Seth C. Rasmussen, Mark M. Richter, Eugene Yi, Helen Place, and Karen J. Brewer*

Received August 3, 1989

A series of bis chelate rhodium(III) and iridium(III) complexes containing polypyridyl bridging ligands have been prepared. Complexes of the type $[Rh(L)_2Br_2]^+$ and $[Ir(L)_2Cl_2]^+$ (where L = 2,2'-bipyrimidine (bpm), 2,3-bis(2-pyridyl)pyrazine (dpp), 2,3-bis(2-pyridyl)quinoxaline (dpq), or 2,3-bis(2-pyridyl)benzoquinoxaline (dpb)) have been prepared, and their syntheses and characterization are reported herein. The complex $[Rh(dpq)_2Br_2](PF_6)\cdot CH_3CN$ and the ligand 2,3-bis(2-pyridyl)quinoxaline have been crystallized and the crystal structures determined. $[Rh(dpq)_2Br_2](PF_6)\cdot CH_3CN$ crystallizes in the triclinic $P\bar{1}$ space group with a = 12.3039 (32) Å, b = 12.8995 (28) Å, c = 13.6792 (34) Å, α = 98.856 (19)°, β = 105.344 (19)°, γ = 107.937 (18)°, Z = 2, R = 0.0773, and R_w = 0.0569. The ligand 2,3-bis(2-pyridyl)quinoxaline crystallizes in the $P2_1/c$ space group with a = 6.2166 (11) Å, b = 15.0398 (30) Å, c = 15.4147 (28) Å, β = 98.911 (15)°, Z = 2, R = 0.0518, and R_w = 0.0436. The electrochemical and spectroscopic properties of these novel bridging ligand complexes differ considerably from those of the previously prepared (2,2'-bipyridine)rhodium and -iridium complexes. All of the bridging ligands used are easier to reduce than bipyridine. Thus, the complexes reported here are easier to reduce and exhibit electronic transitions at lower energy. A number of these new polypyridyl bridging ligand rhodium and iridium complexes catalyze the reduction of carbon dioxide to formate. Remote nitrogens on the polypyridyl bridging ligands make these complexes ideal building blocks for the development of multimetal systems.

Introduction

Although many methods for the electroreduction of CO_2 have been discussed, the vast majority require a large negative potential. In fact, some require potentials far more negative than −2.0 V vs SCE to be effective.[1-3] A promising alternative to direct noncatalyzed reduction of CO_2 at solid electrodes is the use of transition-metal complexes as electrocatalysts.[4-14] One group of electrocatalysts currently being investigated involves d^6 transition metals bound to polypyridyl ligands such as bpy(2,2'-bipyridine).[4,7,8,11,13,14] Metal complexes of polypyridyl ligands are of interest due to their ability to absorb visible light as well as their ability to act as "electron reservoirs".[7,13] Often, these (polypyridyl)metal complexes possess favorable catalytic properties toward CO_2 reduction. One example of such a catalyst is the conpound $[Rh(bpy)_2X_2]X$ (X = Cl^- or $CF_3SO_3^-$).[7,8,11,13] Monometallic complexes like these have been used sucessfully to catalyze the two-electron reduction of carbon dioxide to carbon monoxide and formate.[7,8,11,13]

Two of the most desirable reduction reactions for carbon dioxide are the reductions by six and eight electrons to produce methanol and methane:

$$CO_2 + 6e^- + 6H^+ \rightarrow CH_3OH + H_2O$$

$$CO_2 + 8e^- + 8H^+ \rightarrow CH_4 + 2H_2O$$

Because of the number of electrons needed, such multielectron processes are difficult to achieve with single-metal catalysts. However, it seems possible that multimetal systems would have the possibility of catalyzing these multielectron redox processes due to their ability to store multiple reducing equivalents. With the intention of producing such polymetallic rhodium and iridium compounds, we have synthesized monometallic rhodium and iridium precursor complexes containing polypyridyl bridging ligands. The bridging ligands are similar to bipyridine but have the added ability to coordinate additional metal centers. The structures of the bridging ligands used, 2,2'-bipyrimidine (bpm), 2,3-bis(2-pyridyl)pyrazine (dpp), 2,3-bis(2-pyridyl)quinoxaline (dpq), and 2,3-bis(2-pyridyl)benzoquinoxaline (dpb), are shown as follows:[17,18]

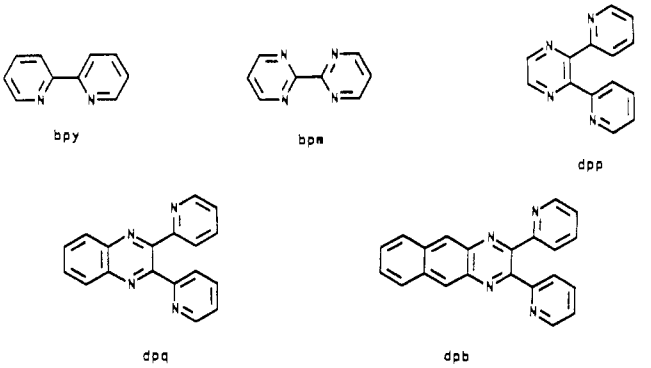

Experimental Section

Materials. Materials were reagent grade and were used without further purification. The rhodium tribromide and iridium trichloride were supplied by Johnson Matthey. 2,3-Bis(2-pyridyl)pyrazine was purchased from Aldrich Chemical Co., and 2,2'-bipyrimidine from Alfa Chemicals.[15] 2,3-Bis(2-pyridyl)quinoxaline was synthesized according to the methods of Goodwin and Lions by the reaction of *o*-phenylenediamine and 2,2'-pyridil in ethanol.[17] 2,3-Bis(2-pyridyl)benzoquinoxaline was synthesized by a modification of the methods of Goodwin and Lions substituting diaminonaphthalene for the *o*-phenylenediamine.[17,18] The ligands dpq and dpb must be recrystallized several times from hot ethanol to remove any unreacted 2,2'-pyridil, which acts as a good ligand and will form complexes with rhodium and iridium.[16] If formed, these complexes are difficult to separate from the desired rhodium and iridium dpq and dpb complexes. The acetonitrile (Burdick and Jackson) used in the electrochemical and spectroscopic studies was spectroquality and was dried over activated molecular sieves. The supporting electroyte was

(1) Amatore, C.; Savent, J.-M. *J. Am. Chem. Soc.* **1981**, *103*, 5021.
(2) Eggins, B. R.; McNeill, J. *J. Electroanal. Chem. Interfacial Electrochem.* **1983**, *148*, 17.
(3) Russell, P. G.; Kovac, N.; Srinivasan, S.; Steinberg, M. *J. Electrochem. Soc.* **1977**, *124*, 1329.
(4) Hawecker, J.; Lehn, J. M.; Ziesser, R. *J. Chem. Soc., Chem. Commun.* **1984**, 328.
(5) Tezuka, M.; Yajima, T.; Tsuchiya, A. *J. Am. Chem. Soc.* **1982**, *104*, 6834.
(6) Beley, M.; Collin, J.-P.; Ruppert, R.; Sauvage, J.-P. *J. Chem. Soc., Chem. Commun.* **1984**, 1315.
(7) Bolinger, C. M.; Sullivan, B. P.; Conrad, D.; Gilbert, J. A.; Story, N.; Meyer, T. J. *J. Chem. Soc., Chem. Commun.* **1985**, 796.
(8) Ayers, W. M. *Catalytic Activation of Carbon Dioxide*; ACS Symposium Series 363; American Chemical Society: Washington, DC, 1986; see also references therein.
(9) Meshitsuka, S.; Ichikawa, M.; Tomaru, K. *J. Chem. Soc., Chem. Commun.* **1974**, 158.
(10) Fisher, B.; Eisenberg, R. *J. Am. Chem. Soc.* **1980**, *120*, 7363.
(11) Collin, J. P.; Sauvage, J. P. *Coord. Chem. Rev.* **1989**, *93*, 245.
(12) Slater, S.; Wagenknecht, J. H. *J. Am. Chem. Soc.* **1984**, *106*, 5367.
(13) Bolinger, C. M.; Story, N.; Sullivan, B. P.; Meyer, T. J. *Inorg. Chem.* **1988**, *27*, 4582.
(14) Sullivan, B. P.; Meyer, T. J. *J. Chem. Soc., Chem. Commun.* **1984**, 403.
(15) Musgrave, F. R.; Westcott, P. A. *Org. Synth.* **1972**, *52*, 1799.
(16) Rasmussen, S. C.; Brewer, K. J. Work in progress.
(17) Goodwin, H. A.; Lions, F. *J. Am. Chem. Soc.* **1959**, *81*, 6415.
(18) Baiano, J. A.; Carlson, D. L.; Wolosh, G. M.; DeJesus, D. E.; Knowles, C. F.; Szabo, E. G.; Murphy, W. R. *Inorg. Chem.*, submitted for publication.

0020-1669/90/1329-3926$02.50/0

electrochemical grade tetrabutylammonium hexafluorophosphate (TBAH) (BioAnalytical Systems) and was stored in a vacuum desiccator. The adsorption alumina used was purchased from Fisher Scientific. All other chemicals were Fisher Scientific reagent grade and were used without further purification.

Syntheses. $[Ir(bpy)_2Cl_2]^+$, $[Rh(bpy)_2Br_2]^+$, and $[Ir(dpp)_2Cl_2]^+$ were prepared according to literature methods.[19-22] $[Rh(en)_2Br_2]Br$ was prepared by a modification of the method Johnson and Basolo used for the preparation of $[Rh(en)_2Cl_2]Cl$ by substituting $RhBr_3 \cdot 3H_2O$ for $RhCl_3 \cdot H_2O$.[23] All other complexes were prepared by modifications of the literature procedure for the synthesis of the dichlorobis(2,3-bis(2-pyridyl)pyrazine)iridium(III) hexafluorophosphate.[19]

Dichlorobis(2,3-bis(2-pyridyl)quinoxaline)iridium(III) Hexaflourophosphate. Preparation of $[Ir(dpq)_2Cl_2](PF_6)$ was achieved by a modification of the procedure for the synthesis of $[Ir(dpp)_2Cl_2](PF_6)$, substituting the ligand dpq (0.55 g, 2.2 mmol) for the ligand dpp. Solid $IrCl_3 \cdot 3H_2O$ (0.24 g, 0.80 mmol) was added to a solution of the ligand dpq (0.55 g, 2.2 mmol) in 70 mL of 2:1 (v/v) ethanol/water. The solution was heated at reflux for ca. 2 h. The ethanol was removed by rotary evaporation. This reaction can also be carried out in 25 mL of ethylene glycol by reducing the heating time to 30 min. Next, a solution of saturated, aqueous KPF_6 (20 mL) was added to the above mixture, an additional 15 mL of water was added, and the yellow-brown solid that formed upon KPF_6(aq) addition was separated by vacuum filtration. The product was washed with 30 mL of 4 °C water. The precipitate was then dissolved in a minimal amount of acetonitrile (10 mL); this solution was filtered and added with stirring to anhydrous diethyl ether (100 mL) to induce precipitation. This precipitate was removed by vacuum filtration and washed with 200 mL of anhydrous diethyl ether. This reprecipitation procedure was repeated twice to remove traces of water or ethylene glycol and excess ligand from the product.

Purification of the product was achieved by column chromatography on adsorption alumina (Fisher Scientific). The yellow-brown precipitate was dissolved in a minimal amount of 3:2 (v/v) toluene/acetonitrile, and the solution was filtered to remove any insoluble material. A 20-cm alumina column was developed with the same solvent mixture. The solution of the crude complex was loaded onto the column and eluted with a 3:2 (v/v) toluene/acetonitrile mixture. The first band eluted was yellow-orange and luminescent. Concentration of this solution by rotary evaporation followed by two repeated chromatography steps yielded the desired product. A typical yield for this reaction was 70%. This complex analyzed well for $[Ir(dpq)_2Cl_2](PF_6)$ (Galbraith Laboratories, Inc.). Anal. Calcd: C, 44.27; Cl, 7.26; H, 2.48. Found: C, 44.25; Cl, 7.35; H, 2.70.

Dichlorobis(2,2'-bipyrimidine)iridium(III) Hexafluorophosphate. $[Ir(bpm)_2Cl_2](PF_6)$ was prepared as above by substituting the ligand bpm (0.356 g, 2.2 mmol) for the ligand dpq. A typical yield for this reaction was 55%. The complex isolated analyzed well for $[Ir(bpm)_2Cl_2](PF_6) \cdot 0.5C_7H_8$. Anal. Calcd: C, 30.39; Cl 9.20; H, 2.09. Found: C, 30.13; Cl, 9.39; H, 2.05.

Dichlorobis(2,3-bis(2-pyridyl)benzoquinoxaline)iridium(III) Hexafluorophosphate. $[Ir(dpb)_2Cl_2](PF_6)$ was prepared as above by substituting the ligand dpb (0.735 g, 2.2 mmol) for the ligand bpm. The reprecipitation technique utilized above was repeated several times to remove ethylene glycol prior to column chromatography. A typical yield was 20%. The complex analyzed well for $[Ir(dpb)_2Cl_2](PF_6) \cdot H_2O$. Anal. Calcd: C, 48.30; Cl, 6.48; H, 2.76. Found: C, 48.54; Cl, 6.82; H, 2.73.

Dibromobis(2,3-bis(2-pyridyl)pyrazine)rhodium(III) Hexafluorophosphate. $[Rh(dpp)_2Br_2](PF_6)$ was prepared as follows. Rhodium(III) tribromide (0.400 g, 1.17 mmol) and the solid ligand, dpp (0.548 g, 2.34 mmol), were dissolved in 40 mL of 2:1 (v/v) ethanol/water and heated at reflux with stirring for 40 min. The solution was filtered hot, and the filtrate was added to the KPF_6 solution prepared by diluting 20 mL of saturated aqueous KPF_6 with 50 mL of water. The resulting bright yellow precipitate was separated from the solution by vacuum filtration and washed with several 30-mL portions of diethyl ether. The product was then purified by alumina chromatography using a 1:1 (v/v) toluene/acetonitrile solvent mixture. The first band eluted was bright yellow. The solution was concentrated by rotary evaporation and added with stirring to 300 mL of diethyl ether to induce precipitation. The precipitate was again separated by vacuum filtration, washed with diethyl ether, and dried under vacuum. This chromatographic procedure was repeated twice to ensure product purity. The final product was recrystallized from hot methanol to produce 0.618 g (0.705 mmol) of purified product. A typical yield for this reaction was 60%. The complex isolated analyzed well for $[Rh(dpp)_2Br_2](PF_6) \cdot H_2O$. Anal. Calcd: C, 37.61; H, 2.48; N, 12.53. Found: C, 38.04; H, 2.53; N, 12.65.

Dibromobis(2,3-bis(2-pyridyl)quinoxaline)rhodium(III) Hexafluorophosphate. $[Rh(dpq)_2Br_2](PF_6)$ was prepared as above by substituting the ligand dpq (0.665 g, 2.34 mmol) for the ligand dpp. The resulting crude product was recrystallized from a hot 2:1 (v/v) toluene/acetonitrile solution to produce 0.720 g (0.724 mmol) of large, square, amber crystals, which were used for X-ray structural analysis. A typical yield for this reaction was 62%. The compound isolated analyzed well for $[Rh(dpq)_2Br_2](PF_6) \cdot CH_3CN$. Anal. Calcd: C, 44.86; H, 2.68; N, 12.39. Found: C, 44.95; H, 2.78; N, 12.00.

Dibromobis(2,2'-bipyrimidine)rhodium(III) Hexafluorophosphate. $[Rh(bpm)_2Br_2]Br$ was prepared previously by Jaradat et al.,[24] but very little characterization data were given. Additionally, no chromatographic procedures were employed to ensure product purity. Elemental analyses were inconsistent with $[Rh(bpm)_2Br_2]Br$. Our synthesis requires chromatographic steps for purification of $[Rh(bpm)_2Br_2](PF_6)$. In our case, $[Rh(bpm)_2Br_2](PF_6)$ was prepared by the procedure used in the preparation of $[Rh(dpp)_2Br_2](PF_6)$, substituting the ligand bpm (0.370 g, 2.34 mmol) for the ligand dpp. Purification of this complex was achieved by alumina chromatography using a 1:1 (v/v) acetonitrile/methanol solvent mixture. This procedure produced 0.391 g (0.540 mmol) of a light yellow solid. A typical yield for this reaction was 46%. The complex isolated analyzed well for $[Rh(bpm)_2Br_2](PF_6) \cdot H_2O$. Anal. Calcd: C, 25.90; H, 1.91; N, 15.09. Found: C, 25.96; H, 2.07; N, 15.29.

Dibromobis(2,3-bis(2-pyridyl)benzoquinoxaline)rhodium(III) Hexafluorophosphate. $[Rh(dpb)_2Br_2](PF_6)$ was prepared and purified as above by substituting the ligand dpb (0.782 g, 2.34 mmol) for the ligand bpm to produce 0.274 g (0.255 mmol) of a dark orange solid. A typical yield for this reaction was 22%. The complex analyzed well for $[Rh(dpb)_2Br_2](PF_6) \cdot H_2O$. Anal. Calcd: C, 48.30; H, 2.76; N, 10.24. Found: C, 48.80; H, 2.84; N, 10.31.

Crystal Growth and Analysis. X-ray-quality crystals of the complex $[Rh(dpq)_2Br_2](PF_6) \cdot CH_3CN$ were obtained by recrystallization from hot 2:1 toluene/acetonitrile by allowing the solution to cool and evaporate in a hood. The large amber crystals obtained in this fashion had the $P\bar{1}$ space group with $a = 12.3039$ (32) Å, $b = 12.8995$ (28) Å, $c = 13.6792$ (34) Å, $\alpha = 98.856$ (19)°, $\beta = 105.344$ (19)°, and $\gamma = 107.937$ (18)°, determined by a least-squares fit of 25 reflections in the range $28° < 2\theta < 32°$. Data were collected at room temperature on a Syntex $P2_1$ instrument (upgraded to Nicolet P3 specifications) with a graphite monochromator and Mo Kα radiation ($\lambda = 0.71069$ Å) using a Wycoff scan with $2\theta = 3$–$45°$. Two standard reflections were monitored every 100 reflections during data collection. The variation of these standard reflections was within counting statistics. An empirical absorption correction was applied. The structure was solved from a Patterson function using SHELXTL 5.1 to find the Rh and Br positions.[25,26] Subsequent difference maps revealed the positions of all other non-hydrogen atoms. Hydrogen atoms were fixed at calculated positions (C–H, N–H = 0.96 Å). A least-squares refinement of 3163 reflections with $F > 3\sigma$ gave $R = 0.0773$ and $R_w = 0.0569$, the function minimized being $\sum w(|F_o| - |F_c|)^2$. The thermal parameters were anisotropic on all non-hydrogen atoms, while hydrogen atom thermal parameters were fixed and approximately 20% larger than those of the corresponding heavy atom.

Crystals of the ligand, 2,3-bis(2-pyridyl)quinoxaline (dpq), were obtained by recrystallization from hot ethanol, allowing the solution to cool and evaporate in the hood. The colorless crystals obtained had the $P2_1/c$ space group determined from the systematic absences $h0l$ (l odd), $0k0$ (k odd), and $00l$ (l odd), with $a = 6.2166$ (11) Å, $b = 15.0398$ (30) Å, $c = 15.4147$ (28) Å, and $\beta = 98.911$ (15)°, based on 25 reflections with $25° < 2\theta < 30°$. Data were collected at room temperature as for the rhodium complex, except no absorption correction was applied. The structure was solved by using direct methods in SHELXTL 5.1.[25,26] Hydrogen atoms were fixed at calculated positions as in the rhodium complex. A least-squares refinement of 1333 reflections with $F > 3\sigma$ gave $R = 0.0518$ and $R_w = 0.0436$. Thermal parameters were anisotropic for all non-hydrogen atoms, with the hydrogen atom thermal parameters fixed as above. Positional and thermal parameters and complete crystallographic data are available as supplementary material.

Spectroscopy. Absorption spectra were recorded on a Hewlett Packard 8452 diode array spectrophotometer (resolution 2 nm) interfaced to a Hewlett Packard Vectra ES computer. Solutions were prepared as

(19) Brewer, K. J.; Petersen, J. D. *Inorg. Chem.*, submitted for publication.
(20) Sofranko, J. A.; Eisenberg, R.; Kampmeier, J. A. *J. Am. Chem. Soc.* **1979**, *101*, 1042.
(21) Gillard, R. D.; Osborn, J. A.; Wilkinson, G. *J. Chem. Soc.* **1965**, 1951.
(22) Watts, R. J.; Crosby, G. A. *J. Am. Chem. Soc.* **1971**, *93*, 3184.
(23) Johnson, S. A.; Basolo, F. *Inorg. Chem.* **1962**, *1*, 925.
(24) Jaradat, Q.; Barqawi, K.; Akasheh, T. S. *Inorg. Chim. Acta* **1986**, *116*, 63.
(25) Sheldrick, G. SHELXTL, Version 5.1: Madison, WI, 1986.
(26) *International Tables for Crystallography*; D. Reidel Publishing Co.: Dordrecht, Holland, 1983; Vol. A.

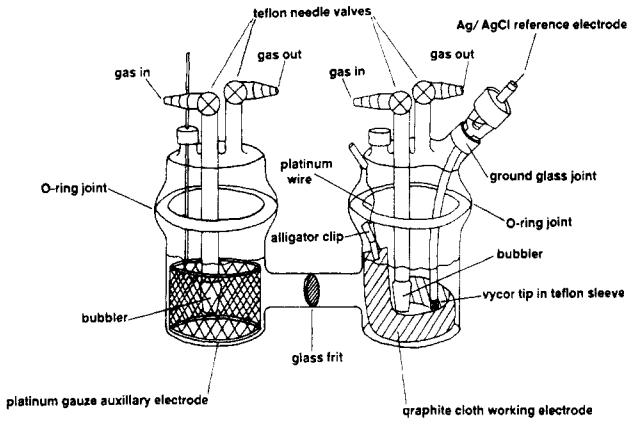

Figure 1. Bulk electrolysis cell used for catalysis studies.

acetonitrile solutions or aqueous solutions of the trifluoromethanesulfonate salt and studied at room temperature. Spectra were displayed on a Hewlett Packard ColorPro plotter.

Emission spectra for the iridium complexes obtained on acetonitrile solutions at room temperature were recorded on a Perkin-Elmer LS-5 fluorescence spectrophotometer and printed on a Perkin-Elmer R100 recorder. Emission spectra for the rhodium complexes were run in the solid state and obtained on a right-angle spectrometer previously described.[27] Samples were placed in a liquid-nitrogen dewar, and the signal was detected with an RCA C31034 photomultiplier tube. All emission spectra are uncorrected.

Electrochemistry. Cyclic voltammograms were recorded on a Bio-Analytical Systems 100A electrochemical analyzer equipped with a Houston Instruments DMP-40 digital plotter. The three-electrode system consisted of a glassy-carbon-disk working electrode, a platinum-wire auxiliary electrode, and a silver/silver chloride gel reference electrode (0.286 V vs SHE). The solvent used was Burdick and Jackson high-purity acetonitrile dried over activated molecular sieves. The supporting electrolyte was 0.1 M TBAH (tetrabutylammonium hexafluorophosphate). The solutions were deoxygenated by bubbling with argon for 20 min prior to each scan and blanketed with argon during the scan. The glassy-carbon working electrode was manually cleaned prior to each individual scan. Peak potentials were reproducible to within ±0.02 V. For experiments run under CO_2, the solutions were saturated with CO_2 by bubbling for 30 min prior to the scan and blanketed with CO_2 during the experiment.

Controlled-potential electrolysis experiments for the electrocatalytic reduction of carbon dioxide were carried out in a gastight three-compartment cell (Figure 1) with a platinum-gauze auxiliary, a graphite-cloth (Electrosynthesis Co.) working, and a Ag/AgCl gel (Bio Analytical Systems) reference electrode. The procedure followed was a modification of that of Meyer.[13]

In a typical experiment, 25, 40, and 3 mL of solution were contained in the working, auxiliary, and reference electrode compartments, respectively. The working and auxiliary compartments were purged with either argon (coulometry) or carbon dioxide (catalysis) for 20 min prior to bulk electrolysis, and the auxiliary compartment was purged with this same gas during the electrolysis. The background current obtained for the solvent and electrolyte at the potential used for the electrolysis was less than 0.2 C. Sufficient amounts of the metal complex being studied were added to the working compartment to achieve a concentration between 2 and 3 mM. For long-term catalysis experiments it was found that the addition of 0.5 mL of water to the auxiliary compartment prevented production of brown species in this area. All electrocatalysis reactions were carried out at a potential of −1.70 V vs Ag/AgCl gel.

Gas Chromatography. Gas chromatographic analyses were carried out on a Gow-Mac Instrument Co. Series 580 gas chromatograph equipped with a thermal conductivity detector and a Spectra-Physics SP4270 integrator/recorder. A molecular sieve column was employed for analysis of gaseous products, while a Porapak Q column equipped with a glass-wool precolumn was used for the analysis of solution products. Helium carrier gas (25 psi) was used in both columns with a flow rate of 79 (molecular sieves) and 100 mL/min (Porapak Q). The column, injection port, and detector temperatures were maintained at 97, 85, and 107 °C, respectively, with a detector current of 150 mA. Gaseous products were analyzed by injecting a 500-μL gas sample into the molecular sieves column. Formate was analyzed by conversion into methyl formate by

Table I. Crystallographic Data for $[Rh(dpq)_2Br_2](PF_6)\cdot CH_3CN$ and 2,3-Bis(2-pyridyl)quinoxaline

chem form	$Rh(C_{18}N_4H_{12})_2Br_2PF_6C_2H_3N$	$C_{18}N_4H_{12}$
fw	1017.39	284.32
space group	$P\bar{1}$	$P2_1/c$
a, Å	12.3039 (32)	6.2166 (11)
b, Å	12.8995 (28)	15.0398 (30)
c, Å	13.6792 (34)	15.4147 (28)
α, deg	98.856 (19)	90
β, deg	105.344 (19)	98.911 (15)
γ, deg	107.937 (18)	90
V, Å^3	1925.22 (78)	1423.82 (47)
Z	2	2
T, °C	25	25
λ, Å	0.71069	0.71069
ρ_{calcd}, g cm^{-3}	1.62	1.32
μ, cm^{-1}	25.94	0.38
transm coeff	0.930–0.739	
$R(F_o)$	0.0773	0.0518
$R_w(F_o)$	0.0569	0.0436

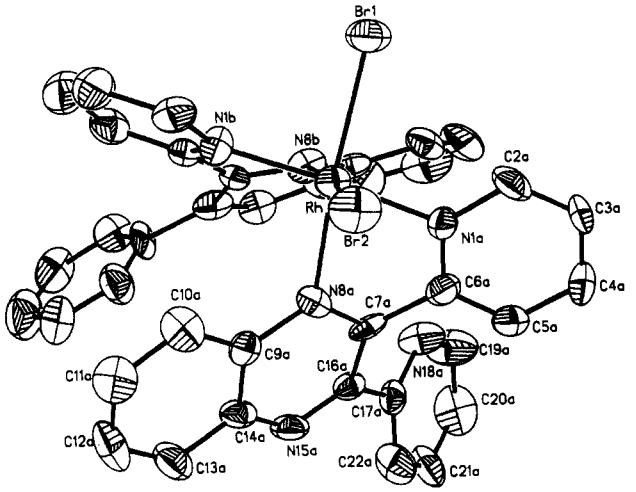

Figure 2. ORTEP diagram of $[Rh(dpq)_2Br_2]^+$.

treatment of 1.0 mL of the electrolyzed solution with excess (ca. 70 mg) $[Me_3O][SbCl_6]$. The amount of methyl formate detected varies with time and reaches a maximum at approximately 35 min following $[Me_3O][SbCl_6]$ addition. Thus, samples were analyzed at this time. A 100-μL sample of the treated solution was injected into the Porapak Q column, and the solution products were detected. Quantitation of the amount of formate present in the electrolyzed samples was achieved by generation of a calibration curve. This curve was obtained by treatment of known formate concentrations with $[Me_3O][SbCl_6]$ and analysis of the methyl formate generated as above at 35 min following treatment.

Results and Discussion

The bridging ligands 2,2′-bipyrimidine, 2,3-bis(2-pyridyl)-pyrazine, 2,3-bis(2-pyridyl)quinoxaline, and 2,3-bis(2-pyridyl)-benzoquinoxaline can be easily substituted for 2,2′-bipyridine in metal complexes by simple modifications of known synthetic procedures.[19-22] The formation of the following bis chelate complexes of iridium(III) and rhodium(III) all occur under relatively mild conditions, and products are isolated in reasonably good yields: $[Ir(bpm)_2Cl_2]^+$, $[Ir(dpp)_2Cl_2]^+$, $[Ir(dpq)_2Cl_2]^+$, $[Ir(dpb)_2Cl_2]^+$, $[Rh(bpm)_2Br_2]^+$, $[Rh(dpp)_2Br_2]^+$, $[Rh(dpq)_2Br_2]^+$, and $[Rh(dpb)_2Br_2]^+$.

The complex $[Rh(dpq)_2Br_2](PF_6)\cdot CH_3CN$ forms large, square, amber crystals upon recrystallization from acetonitrile/toluene. The X-ray crystal structure of the cation $[Rh(dpq)_2Br_2]^+$ is shown in Figure 2. X-ray collection parameters are given in Table I. Atomic coordinates are listed in Table II. Bond angles and bond distances are given in Tables III and IV. All of the rhodium–nitrogen bond lengths are consistent with expected values for coordinated polypyridyl type ligands.[28] Previously, Rillema and

(27) Helms, C. A.; Reynolds, T. A.; Crosby, G. A. *Chem. Phys. Lett.* **1987**, *142*, 99.

(28) Apreda, M. C.; Cano, F. H.; Foces, C.; Haasnoot, J. G.; Prins, R.; Reedijk, J. *Inorg. Chim. Acta* **1986**, *122*, 235.

Table II. Atomic Coordinates ($\times 10^4$) and Isotropic Thermal Parameters ($Å^2 \times 10^3$) for $[Rh(dpq)_2Br_2](PF_6)\cdot CH_3CN$

atom	x	y	z	U^a
Rh	9775 (1)	227 (1)	2472 (1)	31 (1)
Br(1)	11011 (1)	1535 (1)	1717 (1)	50 (1)
Br(2)	10107 (1)	1753 (1)	3957 (1)	52 (1)
N(1a)	11137 (8)	-109 (7)	3404 (7)	32 (4)
C(2a)	12328 (11)	564 (10)	3721 (10)	46 (7)
C(3a)	13175 (11)	221 (2)	4287 (10)	53 (7)
C(4a)	12870 (12)	-797 (13)	4564 (10)	58 (8)
C(5a)	11620 (11)	-1467 (11)	4224 (9)	43 (7)
C(6a)	10782 (11)	-1113 (10)	3633 (9)	37 (6)
C(7a)	9455 (11)	-1661 (9)	3334 (8)	32 (6)
N(8a)	8861 (8)	-1004 (7)	3096 (6)	29 (4)
C(9a)	7658 (11)	-1302 (10)	3101 (8)	34 (6)
C(10a)	7004 (12)	-587 (10)	2956 (9)	45 (7)
C(11a)	5848 (12)	-925 (10)	2987 (10)	51 (7)
C(12a)	5299 (11)	-1995 (11)	3126 (10)	60 (7)
C(13a)	5921 (11)	-2700 (11)	3266 (9)	52 (7)
C(14a)	7106 (11)	-2391 (11)	3242 (9)	38 (6)
N(15a)	7673 (9)	-3132 (8)	3309 (7)	41 (5)
C(16a)	8785 (10)	-2791 (9)	3329 (8)	30 (5)
C(17a)	9300 (11)	-3706 (10)	3253 (10)	36 (6)
N(18a)	10052 (11)	-3660 (9)	2672 (8)	53 (6)
C(19a)	10438 (14)	-4498 (12)	2531 (11)	73 (10)
C(20a)	10122 (13)	-5419 (12)	2944 (12)	73 (9)
C(21a)	9366 (12)	-5460 (12)	3507 (12)	59 (8)
C(22a)	8938 (12)	-4603 (12)	3681 (11)	58 (8)
N(1b)	8308 (8)	360 (8)	1468 (7)	35 (5)
C(2b)	8006 (12)	1273 (11)	1518 (10)	44 (7)
C(3b)	7017 (13)	1259 (12)	748 (12)	58 (9)
C(4b)	6361 (12)	329 (11)	-102 (12)	58 (8)
C(5b)	6649 (11)	-617 (10)	-136 (10)	44 (6)
C(6b)	7650 (11)	-567 (10)	692 (9)	34 (6)
C(7b)	8136 (11)	-1477 (10)	669 (9)	31 (6)
N(8b)	9319 (10)	-1106 (8)	1194 (7)	38 (5)
C(9b)	9942 (12)	-1797 (10)	989 (8)	32 (6)
C(10b)	11224 (12)	-1416 (11)	1383 (9)	44 (7)
C(11b)	11814 (14)	-2093 (15)	1142 (12)	67 (9)
C(12b)	11096 (18)	-3212 (15)	462 (13)	79 (11)
C(13b)	9918 (16)	-3547 (13)	85 (11)	64 (9)
C(14b)	9297 (11)	-2879 (10)	304 (9)	40 (6)
N(15b)	8065 (9)	-3328 (8)	-51 (7)	41 (5)
C(16b)	7478 (12)	-2655 (10)	101 (9)	39 (6)
C(17b)	6137 (11)	-3154 (10)	-169 (11)	43 (6)
N(18b)	5671 (11)	-2806 (10)	530 (8)	53 (6)
C(19b)	4502 (15)	-3323 (13)	324 (12)	64 (9)
C(20b)	3740 (14)	-4180 (14)	-541 (14)	78 (10)
C(21b)	4256 (14)	-4540 (11)	-1254 (12)	66 (8)
C(22b)	5476 (13)	-4039 (10)	-1084 (10)	53 (7)
P(1)	5727 (4)	2535 (4)	3368 (4)	71 (2)
F(1)	5396 (10)	2490 (9)	4370 (8)	152 (7)
F(2)	6025 (12)	2562 (11)	2356 (9)	171 (10)
F(3)	6917 (11)	2412 (17)	3845 (14)	262 (15)
F(4)	6206 (13)	3794 (8)	3653 (10)	192 (9)
F(5)	4462 (10)	2541 (11)	2796 (10)	156 (8)
F(6)	5132 (15)	1245 (9)	3090 (12)	208 (12)
N(3c)	3132 (21)	5365 (21)	2766 (20)	182 (18)
C(2c)	3229 (23)	4880 (22)	3403 (22)	164 (21)
C(1c)	3229 (18)	4197 (15)	4087 (20)	179 (19)

[a] The equivalent isotropic U is defined as one-third of the trace of the orthogonalized U_{ij} tensor.

Table III. Selected Bond Lengths (Å) for $[Rh(dpq)_2Br_2](PF_6)\cdot CH_3CN$

Rh-Br(1)	2.451 (2)	Rh-N(1b)	2.031 (10)
Rh-Br(2)	2.451 (2)	Rh-N(8a)	2.083 (9)
Rh-N(1a)	2.027 (10)	Rh-N(8b)	2.071 (9)

Table IV. Selected Bond Angles (deg) for $[Rh(dpq)_2Br_2](PF_6)\cdot CH_3CN$

Br(1)-Rh-Br(2)	92.0 (1)	Br(1)-Rh-N(1a)	97.2 (3)
Br(2)-Rh-N(8a)	92.5 (1)	N(1a)-Rh-N(8a)	77.2 (4)
N(8a)-Rh-N(8b)	84.6 (4)	N(8a)-Rh-N(1b)	98.1 (4)
N(8b)-Rh-Br(1)	91.4 (3)	N(1b)-Rh-Br(1)	87.0 (3)

co-workers have determined the structure of another dpq complex, namely $[Ru(bpy)_2(dpq)](PF_6)_2$.[29] Comparison of our structure

Table V. Atomic Coordinates ($\times 10^4$) and Isotropic Thermal Parameters ($Å^2 \times 10^3$) for the Ligand 2,3-Bis(2-pyridyl)quinoxaline

atom	x	y	z	U^a
C(5)	3759 (5)	2422 (2)	1041 (2)	49 (1)
C(4)	4358 (5)	2892 (2)	1810 (2)	57 (1)
C(3)	2756 (6)	3326 (2)	2170 (2)	58 (1)
C(2)	645 (6)	3272 (2)	1747 (2)	56 (1)
N(1)	18 (4)	2818 (2)	1002 (2)	48 (1)
C(6)	1585 (4)	2398 (2)	657 (2)	39 (1)
C(7)	836 (4)	1844 (2)	-129 (2)	37 (1)
N(8)	1989 (4)	1125 (2)	-222 (2)	41 (1)
C(9)	1164 (5)	526 (2)	-855 (2)	39 (1)
C(10)	2382 (5)	-226 (2)	-1026 (2)	52 (1)
C(11)	1506 (5)	-836 (2)	-1637 (2)	57 (1)
C(12)	-624 (5)	-740 (2)	-2076 (2)	58 (1)
C(13)	-1825 (5)	-13 (2)	-1935 (2)	51 (1)
C(14)	-929 (5)	648 (2)	-1337 (2)	40 (1)
N(15)	-2035 (4)	1430 (2)	-1285 (2)	44 (1)
C(16)	-1124 (4)	2032 (2)	-726 (2)	36 (1)
C(17)	-2135 (4)	2930 (2)	-798 (2)	39 (1)
N(18)	-763 (4)	3615 (2)	-816 (2)	49 (1)
C(19)	-1651 (6)	4426 (2)	-892 (2)	59 (1)
C(20)	-3825 (6)	4595 (3)	-937 (2)	63 (2)
C(21)	-5219 (6)	3885 (3)	-923 (2)	59 (1)
C(22)	-4374 (5)	3036 (2)	-870 (2)	47 (1)

[a] The equivalent isotropic U is defined as one-third of the trace of the orthogonalized U_{ij} tensor.

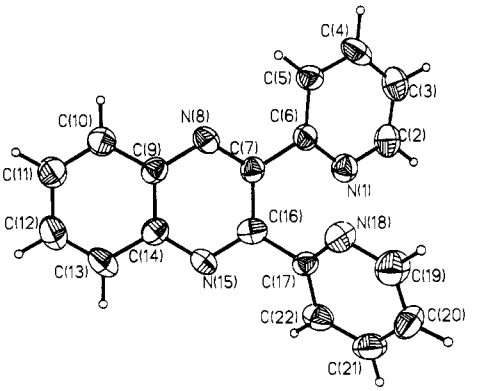

Figure 3. ORTEP diagram of 2,3-bis(2-pyridyl)quinoxaline.

to Rillema's as well as the free dpq ligand structure, shows some quite interesting results. Atomic coordinates for the free dpq ligand are given in Table V.

The Rh-N bond lengths for both bridging ligands are slightly longer for the pyrazine nitrogens (2.083 (9) and 2.071 (9) Å) than for the pyridine nitrogens (2.027 (10) and 2.031 (10) Å). This is expected due to the weaker σ-donor strength of the pyrazine group.[29] This difference in bond lengths for the pyrazine and pyridine M-N bonds could also include contributions due to steric crowding. The bond angles around the rhodium metal center are somewhat distorted from octahedral. Probably the most surprising result of the structural analysis is the conformation of the coordinated dpq ligand.

One might expect that the coordinated pyridine ring would lie in the same plane with the coordinated pyrazine. This is not the case. In fact, coordination of the ligand to the metal center causes only minor changes in the ligand conformation as compared to the free ligand, the ORTEP diagram of which is shown in Figure 3 for comparison. The most notable change in conformation of dpq upon coordination is the "flipping" of one pyridine ring to allow chelation to the metal center (the free ligand has the nitrogens on both pyridine rings rotated toward the center). A significant characteristic of both the bound and the free ligand is the twisting of the pyridine and distortion of the pyrazine rings.

The twisting of the dpq ligand when coordinated to the metal removes some steric crowding. Figure 4 shows a side-on view of

(29) Rillema, D. P.; Taghdiri, D. G.; Jones, D. S.; Keller, C. D.; Worl, L. A.; Meyer, T. J.; Levy, H. A. *Inorg. Chem.* **1987**, *26*, 578.

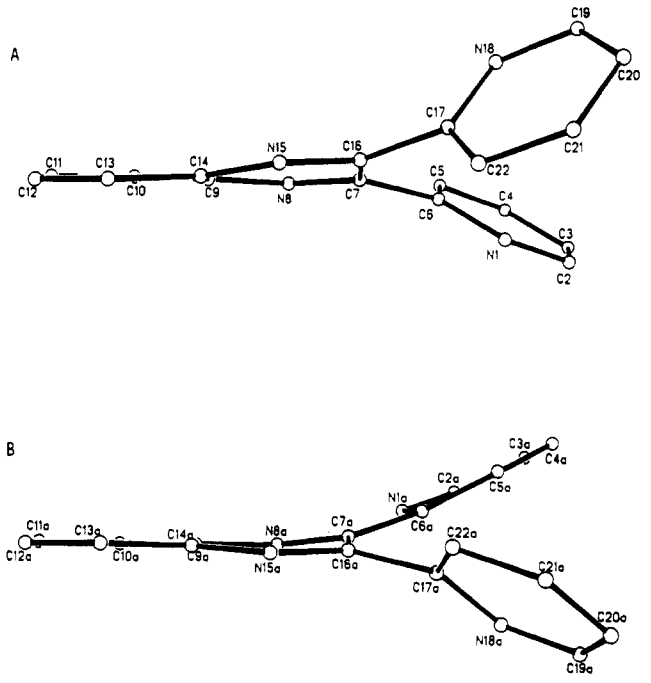

Figure 4. Side-on view of free (A) and coordinated (B) 2,3-bis(2-pyridyl)quinoxaline.

Table VI. Electronic Spectral Data for a Series of Bis Chelate Rhodium(III) Complexes Containing Polypyridyl Bridging Ligands

complex	abs λ_{max}, nm	$10^{-3}\epsilon$, M^{-1} cm^{-1}	em λ_{max}, nm
$[Rh(bpy)_2Br_2]^+$	302	23	660
	311	27	
$[Rh(bpm)_2Br_2]^+$	224	37	691
	328 (sh)	1.0	
$[Rh(dpp)_2Br_2]^+$	280	27	707
	328	19	
$[Rh(dpq)_2Br_2]^+$	256	39	737
	282	32	
	376	11	
$[Rh(dpb)_2Br_2]^+$	334	53	
	408	15	

the free and coordinated ligand. The feature that is immediately obvious from this view is the lack of planarity of the two pyridine rings with each other or with the pyrazine ring. In fact, the torsional angle between the carbon–carbon bonds connecting the pyridine rings to the pyrazine (C(6)–C(7)–C(16)–C(17)) is 30.3 (2)° in the free ligand and 27.5 (1)° in the coordinated ligand. This similarity between the free and the coordinated ligand is quite amazing. Additionally, the pyrazine ring itself is not planar. This ring is distorted from planarity by 8.4° in the free ligand and 7.0° in the coordinated ligand. These distortions from planarity should have a noticeable effect on the electronic communication provided by this bridging ligand. Similar types of distortion are present in Rillema's $[Ru(bpy)_2(dpq)]^{2+}$ system. If these distortions are still present in multimetallic systems, it should limit the amount of electronic communication between the metal centers by lowering the amount of delocalization of electron density over the bridging ligand. Work is currently in progress in our laboratory to synthesize the ligand 4,7-phenanthro[5,6:2',3']quinoxaline (ppq).

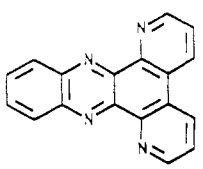

4,7-phenanthro[5,6:2',3']quinoxaline (ppq)

Formation of this carbon–carbon bond between the two 3'-positions on the pyridine rings of the dpq ligand will help minimize the twisting of the pyridine rings and provide better metal–metal communication in multimetallic systems.

Table VII. Electronic Spectral Data for a Series of Bis Chelate Iridium(III) Complexes Containing Polypyridyl Bridging Ligands

complex	abs λ_{max}, nm	$10^{-3}\epsilon$, M^{-1} cm^{-1}	em λ_{max}, nm
$[Ir(bpy)_2Cl_2]^+$	290	27	510
	385	2.8	
	430 (sh)	1.1	
$[Ir(bpm)_2Cl_2]^+$	254	44	525
	332	5.2	
	386	2.0	
	426 (sh)	0.99	
	460 (sh)	<0.20	
$[Ir(dpp)_2Cl_2]^+$	230	31	562
	276	34	
	320	23	
	406	2.0	
	480 (sh)	<0.20	
$[Ir(dpq)_2Cl_2]^+$	218	38	634
	276	34	
	372	13	
	460	3.4	
	514	1.2	
$[Ir(dpb)_2Cl_2]^+$	208	85	
	260	75	
	328	43	
	408	10	
	528	2.0	

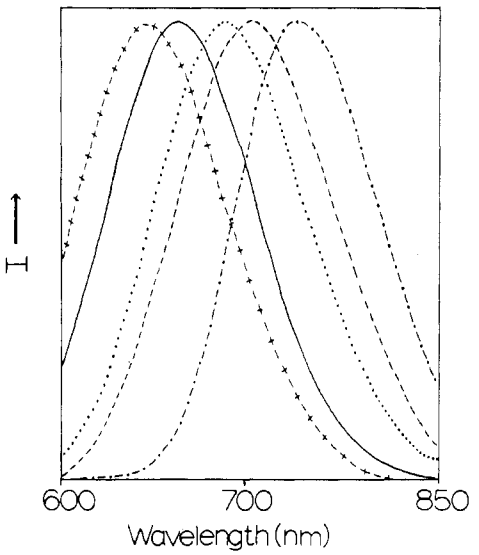

Figure 5. Emission spectra for a series of rhodium(III) bis chelate polypyridyl complexes: (−+−) $[Rh(en)_2Br_2]Br$; (—) $[Rh(bpy)_2Br_2]Br$; (···) $[Rh(bpm)_2Br_2]Br$; (- - -) $[Rh(dpp)_2Br_2]Br$; (-·-) $[Rh(dpq)_2Br_2]Br$.

Tables VI and VII summarize the electronic spectral data for this new series of rhodium(III) and iridium(III) bridging ligand complexes as well as the previously prepared bpy complexes.[22,30-32] The absorption spectra are dominated by intense ligand-based bands in the ultraviolet region, while charge-transfer bands are observed in the visible. The spectra of all of the rhodium bridging ligand complexes have tails well into the visible region of the spectrum. Location of peak maxima in this region is difficult, and thus no values are reported. Since all of the bridging ligands are easier to reduce than bpy, the substitution of these bridging ligands for bpy results in a shift to lower energy of the charge-transfer transitions as expected. This shift is even more evident in the emission spectra.

Although the iridium complexes emitted at room temperature in fluid solution, the rhodium complexes only showed emission

(30) Crosby, G. A. *Acc. Chem. Res.* **1975**, *8*, 231.
(31) Watts, R. J. *Inorg. Chem.* **1981**, *20*, 2302.
(32) Kahl, J. L.; Hanck, W.; DeArmond, M. K. *J. Phys. Chem.* **1978**, *82*, 540.

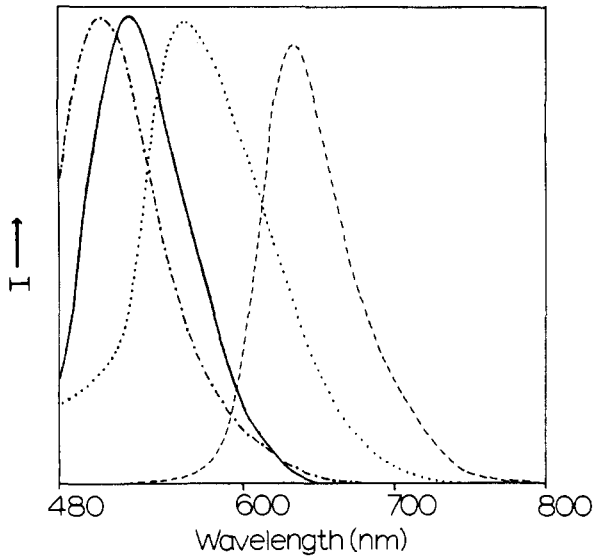

Figure 6. Emission spectra for a series of iridium(III) bis chelate polypyridyl complexes: (-·-) $[Ir(bpy)_2Cl_2](PF_6)$; (—) $[Ir(bpm)_2Cl_2](PF_6)$; (···) $[Ir(dpp)_2Cl_2](PF_6)$; (- - -) $[Ir(dpq)_2Cl_2](PF_6)$.

Table VIII. Cyclic Voltammetric Data for Rhodium Polypyridyl Complexes

complex	E_p^a, V	E_p^c, V	$E_{1/2}$, V
$[Rh(bpy)_2Br_2]^+$		-0.79	
	-1.26	-1.33	-1.30
	-1.46	-1.54	-1.50
$[Rh(bpm)_2Br_2]^+$		-0.62	
		-1.34	
		-1.70	
$[Rh(dpp)_2Br_2]^+$		-0.60	
	-0.99	-1.10	-1.05
	-1.15	-1.23	-1.19
$[Rh(dpq)_2Br_2]^+$		-0.44	
	-0.74	-0.96	-0.85
	-1.37	-1.60	-1.49
$[Rh(dpb)_2Br_2]^+$		-0.39	
	-0.68	-0.77	-0.72
	-1.18	-1.30	-1.24

as solids at 77 K. Figures 5 and 6 illustrate the emission spectra for this new series of complexes. No emission could be detected under our conditions for either the rhodium or the iridium dpb system, probably due to the low red sensitivity of the photomultiplier tubes used to detect the emission. Since rhodium(III) is easier to reduce than iridium(III), one would expect the rhodium complexes to emit at lower energy than the analogous iridium complexes. In fact, one would expect that the lowest energy excited state in the rhodium complexes would be a ligand field state (as illustrated by the 641-nm emission of $[Rh(en)_2Br_2]^+$, which has no ligand π^* orbitals), while that of the iridium complexes is expected to be a metal-to-ligand charge-transfer state. Furthermore, one would expect the trend in emission maxima for complexes of each metal to follow the reduction potential of the ligands, which become easier to reduce in the series bpy < bpm < dpp < dpq < dpb.[17,18,29,33] As shown in Figures 5 and 6, the emission maxima decrease in energy from $[Ir(bpy)_2Cl_2]^+$ to $[Ir(bpm)_2Cl_2]^+$, $[Ir(dpp)_2Cl_2]^+$, $[Ir(dpq)_2Cl_2]^+$, $[Rh(bpy)_2Br_2]^+$, $[Rh(bpm)_2Br_2]^+$, $[Rh(dpp)_2Br_2^+]$, and $[Rh(dpq)_2Br_2]^+$. This is consistent with the expected behavior for the substitution of the progressively easier to reduce bridging ligands for bipyridine. Remarkably, the substitution of dpq for bpy results in a 124-nm shift in the emission maxima for the iridium(III) complexes. Thus, the incorporation of these polypyridyl bridging ligands into a metal framework is useful not only in that it makes possible the development of multimetal systems but also in that it shifts the absorption and emission maxima to lower energy.

Table IX. Cyclic Voltammetric Data for Iridium Polypyridyl Complexes

complex	E_p^a, V	E_p^c, V	$E_{1/2}$, V
$[Ir(bpy)_2Cl_2]^+$	-1.10	-1.25	-1.18
	-1.30	-1.47	-1.39
		-2.12	
$[Ir(bpm)_2Cl_2]^+$	-0.73	-0.79	-0.76
	-0.89	-0.97	-0.93
		-1.65	
$[Ir(dpp)_2Cl_2]^+$	-0.80	-0.86	-0.83
	-1.03	-1.09	-1.06
		-1.75	
$[Ir(dpq)_2Cl_2]^+$	-0.44	-0.50	-0.47
	-0.62	-0.70	-0.66
		-1.50	
$[Ir(dpb)_2Cl_2]^+$	-0.27	-0.39	-0.33
	-0.50	-0.60	-0.55
		-1.34	

Tables VIII and IX summarize the electrochemical data for this series of complexes. Electrochemically, the rhodium complexes behave quite differently from the iridium complexes. Rhodium is easier to reduce than iridium. In all of the rhodium complexes prepared, the first reduction is an irreversible metal-centered reduction, followed by successive ligand-based reductions.[13,34] In analogy to the previously studied $[Rh(bpy)_2Cl_2]^+$, as illustrated by the work of DeArmond and co-workers,[32] the electrochemical processes observed for the series of rhodium bridging ligand complexes can be described as follows:

$$[Rh(BL)_2Br_2]^+ \underset{2e^-}{\overset{2e^-}{\rightleftharpoons}} [Rh(BL)_2Br_2]^-$$

$$[Rh(BL)_2Br_2]^- \xrightarrow{fast} [Rh(BL)_2]^+ + 2Br^-$$

$$[Rh(BL)_2]^+ \underset{1e^-}{\overset{1e^-}{\rightleftharpoons}} [Rh(BL)_2]$$

$$[Rh(BL)_2] \underset{1e^-}{\overset{1e^-}{\rightleftharpoons}} [Rh(BL)_2]^-$$

In the bpm case, the ligand reductions are largely irreversible, and thus no anodic peak potentials are reported.

In the iridium complexes, the first two reductions are ligand-based reductions followed by a metal-based reduction of the iridium:[19,35]

$$[Ir(BL)_2Cl_2]^+ \underset{1e^-}{\overset{1e^-}{\rightleftharpoons}} [Ir(BL)_2Cl_2]$$

$$[Ir(BL)_2Cl_2] \underset{1e^-}{\overset{1e^-}{\rightleftharpoons}} [Ir(BL)_2Cl_2]^-$$

$$[Ir(BL)_2Cl_2]^- \underset{2e^-}{\overset{2e^-}{\rightleftharpoons}} [Ir(BL)_2Cl_2]^{3-}$$

$$[Ir(BL)_2Cl_2]^{3-} \xrightarrow{fast} [Ir(BL_2)]^- + 2Cl^-$$

As expected, the substitution of either bpm, dpp, dpq, or dpb for bpy in this series of bis chelate iridium complexes results in systems that are progressively easier to reduce. In fact, $[Ir(dpb)_2Cl_2]^+$ is easier to reduce by 0.85 V than the analogous $[Ir(bpy)_2Cl_2]^+$.

An additional consequence of the ease of reduction of these bridging ligand is the stability of the one- and two-electron-reduction products of $[Ir(bpm)_2Cl_2]^+$, $[Ir(dpp)_2Cl_2]^+$, $[Ir(dpq)_2Cl_2]^+$, and $[Ir(dpb)_2Cl_2]^+$. $[Ir(bpy)_2Cl_2]^+$ can be reduced reversibly at very high scan rates to both $[Ir(bpy)_2Cl_2]$ and $[Ir(bpy)_2Cl_2]^-$. At slow scan rates (<3000 mV/s), both of these reductions are irreversible due to thermal population of a metal-centered state, which results in Cl^- loss.[19,32] Both the first and second reductions of $[Ir(bpm)_2Cl_2]^+$, $[Ir(dpp)_2Cl_2]^+$, $[Ir(dpq)_2Cl_2]^+$, and $[Ir(dpb)_2Cl_2]^+$ are completely reversible (ΔE_p = 59 mV, i_p^c/i_p^a =

(33) Braustein, C. H.; Baker, A. D.; Strekas, T. C.; Gafney, H. D. *Inorg. Chem.* **1984**, *23*, 857.

(34) Kew, G.; DeArmond, K.; Hanck, K. *J. Phys. Chem.* **1974**, *78*, 727.

(35) DeArmond, K.; Hillis, J. *J. Chem. Phys.* **1971**, *54*, 2247.

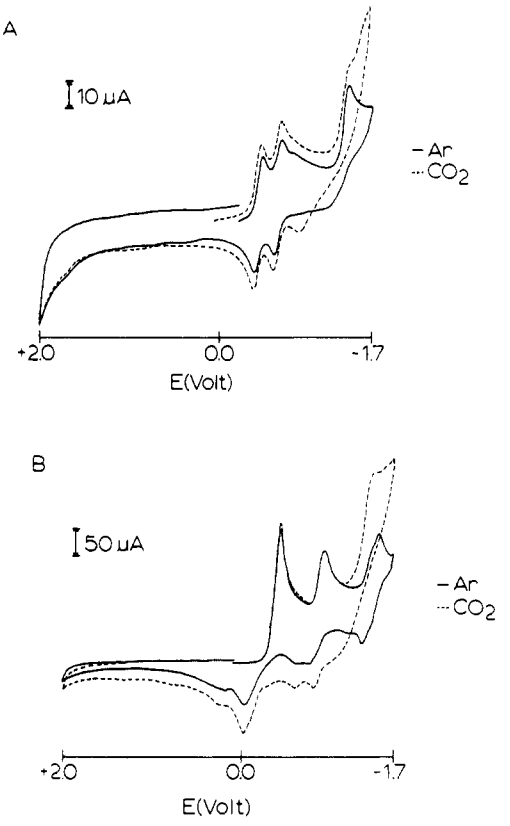

Figure 7. Cyclic voltammograms of $[Ir(dpq)_2Cl_2]^+$ (A) and $[Rh(dpq)_2Br_2]^+$ (B) in CH_3CN/0.1 M TBAH.

1.0) at scan rates above 10 and 500 mV/s for the first and second reductions, respectively. This difference in reversibility is attributed to a lowering in energy of the ligand-based orbitals in the bridging ligand complexes significantly below the metal-based orbitals, preventing thermal population of the metal-based orbitals. Since it is these thermally populated metal-based orbitals that are responsible for loss of Cl^-, the bridging ligand complexes are more stable in the reduced form.

Figure 7 shows the cyclic voltammograms of $[Ir(dpq)_2Cl_2]^+$ and $[Rh(dpq)_2Br_2]^+$. The solid lines illustrate the electrochemical behavior under argon, while the dashed lines show the behavior under CO_2. Background current for the bare electrode under either argon or carbon dioxide is negligible in this potential window and is omitted for clarity. Under argon, the iridium complex exhibits two reversible ligand-based reductions ($E_{1/2}$ = −0.47 and −0.66 V vs Ag/AgCl) followed by an irreversible metal-based reduction with E_p^c = −1.50 V. Under similar conditions the rhodium dpq complex shows an irreversible metal-based reduction with E_p^c = −0.44 V followed by two quasi-reversible ligand-based reductions with half-wave potentials of −0.85 and −1.49 V. Both complexes exhibit different electrochemical behavior under a carbon dioxide atmosphere. An increase in cathodic current is obtained as well as a loss of reversibility and a decrease in anodic current. This behavior is quite similar to that of $[Rh(bpy)_2(TFMS)_2]^+$ (TFMS = trifluoromethanesulfonate), which is known to catalyze the reduction of carbon dioxide to carbon monoxide and formate.[7]

Carbon dioxide reduction catalysis experiments have been performed on this series of new rhodium and iridium complexes, and the results are summarized in Table X. In all of the catalysis experiments performed, the current dropped slightly during the first 10–20 min and remained fairly constant (±25%) following that time with a much slower decline over the rest of the experiment. Typically, electrocatalysis was carried out for 100–140 min. The total current reported in Table X represents all current passed by the electrode. The HCO_2^- current is determined by detection of methyl formate produced from the conversion of HCO_2^- to HCO_2CH_3 by reaction with excess $[Me_3O][SbCl_6]$. Realizing the production of HCO_2^- requires $2e^-$, the current can be calculated. The current efficiency for formate production is given in parentheses following the HCO_2^- current. Turnovers reported are for the production of HCO_2^- only.

Table X. Electrocatalytic Reduction of Carbon Dioxide in CH_3CN[a]

catalyst	total current,[b] C	HCO_2^- current[c] C (efficiency, %)	turnovers[d]
$[Rh(bpm)_2Br_2]^+$	78.4	43.9 (63.3)	4.8
$[Rh(dpp)_2Br_2]^+$	98.4	46.3 (51.7)	5.3
$[Rh(dpq)_2Br_2]^+$	60.1	36.7 (70.3)	4.6
$[Rh(dpb)_2Br_2]^+$	82.2	14.5 (18.8)	3.0
$[Ir(bpm)_2Cl_2]^+$	32.5	13.5 (55.1)	2.1
$[Ir(dpp)_2Cl_2]^+$	71.0	18.3 (28.3)	2.9
$[Ir(dpq)_2Cl_2]^+$	52.1	15.0 (32.5)	2.6
$[Ir(dpb)_2Cl_2]^+$	58.6	16.2 (30.6)	2.8

[a] Experiments were carried out in CH_3CN saturated with carbon dioxide with 0.1 M TBAH electrolyte and 2–3 mM added metal catalyst. [b] Total current passed by the electrode. [c] Amount of current attributed to formate production, determined as methyl formate. [d] Turnovers for the production of formate only.

All of the complexes studied catalyzed the reduction of carbon dioxide to formate. As pointed out in an earlier study by Meyer,[13] the protons needed for the production of the observed reduction products can be obtained from the supporting electrolyte via the Hofmann degradation. As can be seen in Table X, all of the rhodium complexes with the exception of $[Rh(dpb)_2Br_2]^+$ have current efficiencies of >50% for the production of formate. In fact, these systems mimic the activity of $[Rh(bpy)_2(TFMS)_2]^+$ quite well. It is interesting to note that substitution of the polypyridyl bridging ligands bpm, dpp, and dpq for bpy have very little effect on the catalytic activity of the complex. Additionally, one of the iridium systems studied, namely $[Ir(bpm)_2Cl_2]^+$, gives good current efficiency (55.1%) for the production of formate. All of the other iridium complexes have lower current efficiencies, 28.3–32.5%. This lowering of the efficiency for the production of formate could be due to the formation of some other CO_2 reduction product not detected in this study. The catalytic behavior exhibited by these new rhodium and iridium complexes is quite similar to that reported for the previously studied bipyridine complexes[13] and indicates that substitution of these bridging ligands for bipyridine on these catalytically active metals can be achieved without loss of catalytic activity.

The bis-chelated rhodium(III) and iridium(III) bridging ligand complexes can be prepared under relatively mild conditions. The substitution of these bridging ligands for 2,2′-bipyridine produces complexes with electronic transitions that occur at lower energy and reductions that occur at lower potential. These characteristics may be useful in solar energy conversion schemes as well as electrocatalysis. Substitution of these bridging ligands for bipyridine does not significantly alter the desired catalytic activity of the metal. In addition, the presence of the remote nitrogens made available through the incorporation of the bridging ligands makes possible the development of multimetal systems.[16] These multimetal systems should have unusual photophysical properties as well as the interesting reactivity with carbon dioxide.

Acknowledgment. We thank Dr. Glenn Crosby, Tom Reynolds, and Durwin Striplin for their help in obtaining the solid-state emissions for the rhodium complexes. Support of the NSF (Grant CHE-8408407) and the Boeing Co. for the purchase of the X-ray diffractometer system is acknowledged. Special thanks are expressed to Prof. Roger Willett for his assistance with the interpretation of the Patterson function and to Bill Ryan for the construction of the electrocatalysis cell. We also thank Johnson Matthey for the loan of the rhodium and iridium metals used in these studies. This investigation was supported in part by funds provided by Washington State University.

Supplementary Material Available: Tables SI–SIX, giving X-ray data collection parameters, bond lengths and angles, anisotropic thermal parameters, and H atom coordinates, and Figures S1 and S2, showing packing diagrams (13 pages); Tables SX and SXI, listing calculated and observed structure factors (40 pages). Ordering information is given on any current masthead page.